IOP Publishing Physica Scripta
Phys. Scr. 95 (2020) 065403 (12pp) https://doi.org/10.1088/1402-4896/ab725e

Electron capture by fast projectiles from lithium, carbon, nitrogen, oxygen and neon

I Mančev[1], N Milojević[1], D Delibašić[1] and Dž Belkić[2,3]

[1] Department of Physics, Faculty of Sciences and Mathematics, University of Niš, PO Box 224, 18000 Niš, Serbia
[2] Karolinska Institute, Department of Oncology-Pathology, PO Box 260, SE-171 76, Stockholm, Sweden
[3] Radiation Physics and Nuclear Medicine, Karolinska University Hospital, SE-171 76 Stockholm, Sweden

E-mail: mancev@pmf.ni.ac.rs

Received 3 October 2019, revised 6 January 2020
Accepted for publication 3 February 2020
Published 20 March 2020

Abstract

The three-body boundary-corrected continuum intermediate state method is used to compute total cross sections for single charge exchange in ion-atom collisions at intermediate and high impact energies. Detailed illustrations are given for several scattering systems: $H^+ + Li$, $He^{2+} + Li$, $H^+ + C$, $He^{2+} + C$, $H^+ + N$, $H^+ + O$ and $H^+ + Ne$, $He^{2+} + Ne$. An independent particle model and the frozen-core approximation are employed with only one target electron taken as being active. The initial ground state of the active electron in a multi-electron target is described by five wave functions. These are two Roothaan-Hartree-Fock (RHF) wave functions, the single- as well as double-zeta functions and the hydrogen-like functions. Comparisons among the resulting cross sections are made to check their sensitivity to the choice of the initial target wave functions. In the case of a lithium target, the separate cross sections for electron capture from the K-shell and L-shell are reported. The present theoretical total cross sections are compared with the available experimental data and overall good agreement is found, especially when using the RHF wave functions for multi-electron targets.

Keywords: fast ion atom collision, electron capture, charge exchange

1. Introduction

Over the years, charge exchange in energetic collisions between heavy ions (bare or electron bearing) and multi-electron atoms has received much attention from both theoretical and experimental standpoints [1–47]. These processes (also known as electron capture or electron transfer) find important applications in basic and applied sciences across interdisciplinary fields (plasma physics, astrophysics, surface physics, medical physics, hadron therapy, etc). Also a notable role of charge exchange is for plasma diagnostics (line emissions) in thermonuclear fusion research.

In general, various existing theoretical methods can yield reliable cross sections for electron transfer depending on impact energies. At higher impact energies, charge exchange can reliably be described by these methods: the continuum distorted wave (CDW) [1], the boundary-corrected continuum intermediate state (BCIS) [19, 46], the first Born with correct boundary conditions (CB1) [8, 12–15, 17, 18], the second Born with correct boundary conditions (CB2) [16], their hybrids and other perturbative methods reviewed in [4]. In particular, the presently used three-body version of the BCIS method is an appropriate adaptation [46] of the earlier introduced and implemented four-body variant of this theory for double electron capture [19].

At lower and intermediate impact energies, the expansion methods of the close-coupling type are appropriate using atomic and/or molecular basis set functions. Such formalisms are various adiabatic, hyperspherical, and molecular-orbital close-coupling methods [48, 49]. Electron capture, excitation and ionization can also be described by the three variants of the convergent close coupling (CCC) methods: the quantum-mechanical (QM-CCC) [50], the semi-classical (SC-CCC) [51] and the wave-packet (WP-CCC) [52, 53]. For example, algorithmically, the QM-CCC method involves the coupled-channel Lippmann-Schwinger equations for the transition amplitudes in the momentum-space. With sufficiently large sets of the expansion functions, the CCC methods can comprehensively cover not only lower and intermediate, but also higher impact energies.

Theories for describing single charge exchange in collisions of e.g. bare ions with multi-electron atoms are usually formulated by means of the independent particle model.

Herein, only the electron to be transferred is considered as active. In such a case, the transition amplitudes (prior and post) deal explicitly with the wave functions and the perturbation potentials of the active electron alone. In these T-matrix elements, except for a screening effect, there is no trace whatsoever from the remaining electrons of the given multi-electron atomic target. The only role of the non-participating (passive) electrons is to merely screen the target nuclear charge seen by the active electron and the projectile nucleus. For this to occur, an additional assumption is necessary. It is called the frozen-core approximation which assumes that all the passive electrons occupy the same orbitals before and after the collision.

The simplest manner to describe the ground state of a multi-electron target is to use a screened nuclear charge and the hydrogen-like wave function for the active electron. A physically more satisfactory approach is to utilize the Hartree-Fock (HF) wave functions for multi-electron atomic targets. Among the HF wave functions, the most convenient are those represented by certain closed forms. Such are the Roothan-Hartree-Fock (RHF) wave functions [54, 55] available as the analytical expressions. The most frequently employed RHF wave functions are those from [56] given by linear combinations of the Slater-type orbitals (STOs). All the needed coefficients in these linear combinations are listed in [56] for many elements of the periodic table.

This makes the efforts in the calculations of the T-matrix elements with the RHF wave function [56] comparable to those with the hydrogen-like wave functions. The main difference is that, for the given transition, there are more integrals to calculate with the RHF than with the hydrogen-like wave function. However, all the integrals with the RHF wave functions in the T-matrix elements are of the same typical forms as those employing the hydrogen-like wave functions. This is due to the said STO basis set in the analytical RHF wave functions [56]. As is well-known, even the hydrogen-like wave function itself can be expressed as a sum of the STOs.

The systematic use of the RHF model for one electron capture by bare or dressed ions from multi-electron targets has been suggested in [8] with the illustrations in the CDW method [1]. Thus, in [8], for e.g. bare ions as projectiles, a purely Coulombic target potential has been employed together with the RHF binding energy and the RHF wave function from [56] for the initial orbital of the active electron. For a multi-electron atomic system, the RHF orbital energy (as computed by means of the self-consistent-field method) is known to be generally in close agreement with the corresponding experimental binding energies. However, this does not automatically imply that the resulting cross sections would also be adequate. Therefore, explicit computations are desirable to test the sensitivity of the cross sections to different choices of the target wave functions and the corresponding binding energies of the ground-states of multi-electron targets. Here, we shall accomplish this task by using the available two RHF functions [56–59], the single- and double-zeta functions [56], as well as the hydrogen-like wave functions.

The present study is concerned with charge exchange in several collisions such as $H^+ + Li$, $He^{2+} + Li$, $H^+ + C$, $He^{2+} + C$, $H^+ + N$, $H^+ + O$, $H^+ + Ne$ and $He^{2+} + Ne$. Computations of total cross sections are carried out by means of the BCIS method in its three-body formulation. Note that, as opposed to the symmetric treatment of both channels in the three-body CDW method, the formalism of the BCIS method is asymmetric. It involves only one electronic Coulomb wave function in either the entrance or exit channel wave functions for the post or prior form of the transition amplitudes, respectively. We employ the independent particle model and the mentioned five different wave functions of the considered ground-state target systems. Thorough comparisons of the obtained results with the available experimental data are performed, and the validity of the BCIS method is thereby assessed.

Atomic units will be used throughout unless otherwise stated.

2. Theory

We begin by considering charge exchange between a completely stripped projectile (P) and a neutral multi-electron target atom (T) of nuclear charge Z_P and Z_T, respectively:

$$Z_P + T(i) \longrightarrow (Z_P, e)_f + T^+. \tag{1}$$

The independent particle model will be used in which, as stated, only the electron to be captured is considered as active. Moreover, this is the only electron which explicitly appears throughout the formalism. The remaining, non-captured electrons are viewed as passive in the sense that they occupy the same orbitals before and after the collision (the so-called frozen-core approximation) [8].

Index i in $T(i)$ from (1) denotes the initial orbital of the target atom from which the active electron is to be captured. As a consequence of the frozen-core approximation, the final state of the target T^+ does not intervene at all in the single-particle formalism. Let $\vec{s}$ ($\vec{x}$) be a position vector of the electron relative to the projectile (target nucleus), respectively. Further, let $\vec{R}$ denotes the position vector of the projectile with respect to the target nucleus. The initial and final unperturbed states are $\Phi_i = e^{i\vec{k}_i\cdot\vec{r}_i}\varphi_i(\vec{x})$ and $\Phi_f = e^{-i\vec{k}_f\cdot\vec{r}_f}\varphi_f(\vec{s})$ where $\vec{k}_i$ and $\vec{k}_f$ are the initial and final momentum, respectively. Here, $\vec{r}_i$ $\{\vec{r}_f\}$ is the position vector of Z_P $\{Z_T\}$ relative to $T(i)$ $\{(Z_P, e)_f\}$.

The prior form of the transition amplitude for process (1) in the BCIS method can be represented by the following six-dimensional integral [46]:

$$\begin{aligned} T_{if}(\vec{\eta}) = [N^-(\nu_T)]^* \int\int d\vec{s}\, d\vec{R}\, \varphi_f^*(\vec{s}) \\ \times \left(\frac{Z_P}{R} - \frac{Z_P}{s}\right)\varphi_i(\vec{x})\, e^{i\vec{\beta}\cdot\vec{R} - i\vec{v}\cdot\vec{s}} \\ \times {}_1F_1(i\nu_T, 1, ivx + i\vec{v}\cdot\vec{x}) \\ \times (\rho v)^{2iZ_P(Z_T^{\rm eff}-1)/v}(vR + \vec{v}\cdot\vec{R})^{i\xi}, \end{aligned} \tag{2}$$

where $\vec{v}$ is the incident velocity vector along the $Z-$axis and $\vec{\rho}$ is the vectorial component of $\vec{R}$ in the XOY-plane ($\vec{\rho}\cdot\vec{v} = 0$). Further, $N^-(\nu_T) = e^{\pi\nu_T/2}\,\Gamma(1 + i\nu_T)$, $\nu_T = Z_T^{\rm eff}/v$, $\xi = Z_P/v$ and $Z_T^{\rm eff}$ is the target effective nuclear charge. Here, Γ is the

standard gamma function and ${}_1F_1(a, b, z)$ is the regular confluent hypergeometric (Kummer) function. The wave function of the hydrogen-like system $(Z_P, e)_f$ in the exit channel is denoted by $\varphi_f(\vec{s})$ and its corresponding binding energy is E_f. Function $\varphi_i(\vec{x})$ represents the initial bound-state wave function of the active electron in the multi-electron target T(i) with the binding energy $E_i^{\rm RHF}$. The exponential $e^{i\vec{\beta}\cdot\vec{R}-i\vec{v}\cdot\vec{s}}$ in (2) comes from the eikonal approximation $\vec{k}_i\cdot\vec{r}_i+\vec{k}_f\cdot\vec{r}_f\approx\vec{\beta}\cdot\vec{R}-\vec{v}\cdot\vec{s}$, where $\vec{\beta}$ is the momentum transfer vector $\vec{\beta}=-\vec{\eta}-(v/2+\Delta E/v)\hat{\vec{v}}$ with $\Delta E=E_i^{\rm RHF}-E_f$ and $\hat{\vec{v}}=(1/v)\vec{v}$. Moreover, $\vec{\eta}$ is the transverse momentum transfer vector $\vec{\eta}=(\eta\cos\phi_\eta, \eta\sin\phi_\eta, 0)$ which is perpendicular to $\vec{v}$, so that $\vec{\eta}\cdot\vec{v}=0$.

In the prior form of the BCIS method, the intermediate channel for describing transient ionization of the captured electron in the exit channel is included in the same way as in the corresponding CDW method [1, 8]. These two treatments differ in the entrance channel of the prior transition amplitude, where the BCIS method employs the total scattering wave function of the boundary-corrected first Born (CB1) method [8, 12].

The physical interpretation of the prior form of the T-matrix element in the BCIS method runs as follows. In the entrance channel, the impinging projectile Z_P interacts with $(Z_T^{\rm eff}, e)_i$ through the asymptotic residual Coulomb potential $Z_P(Z_T^{\rm eff}-1)/R$. Such a circumstance leads to the compound or collective logarithmic Coulomb phase factor $D_i(\vec{R})=\exp[(i/v)Z_P(Z_T^{\rm eff}-1)\ln(vR-\vec{v}\cdot\vec{R})]$ as the sole modification of the initial unperturbed state Φ_i. This is the phase for the entire colliding system (projectile-target or aggregate-aggregate) and, therefore, it does not include the modifying factor due to the explicit electronic motion in the Coulomb field of the nuclear charge Z_P.

Contrary to this, in the exit channel, the BCIS method allows the scattered projectile to perturb separately the nuclear and electronic motions. Therein, the repulsive Coulomb interaction between nuclear charges Z_P and $Z_T^{\rm eff}$ yields the nucleus-nucleus phase factor $D_f(\vec{R})=\exp[-(i/v)Z_PZ_T^{\rm eff}\ln(vR+\vec{v}\cdot\vec{R})]$. Simultaneously, the Coulomb interaction of Z_P with the active electron e leads to transient ionization of the target system $(Z_T^{\rm eff}, e)$. This is a continuum intermediate state of the electron in the field of its parent nucleus of charge $Z_T^{\rm eff}$. In the BCIS method, the ejected electron does not propagate in the Coulomb field of the point charge $Z_T^{\rm eff}$ with a whole spectrum of possible momenta $\vec{k}$. Rather, this method (similarly to the CDW method) imposes the specific velocity matching condition which constrains the free electron to travel only in a restricted direction with the particular momentum $\vec{k}=\vec{v}$. Such an imposition produces the explicit purely electronic modifying factor $d_f(\vec{x})=e^{-i\vec{v}\cdot\vec{x}}\varphi_{\vec{v}}^-(\vec{x})$ where $\varphi_{\vec{v}}^-(\vec{x})=N^-(\nu_T)e^{i\vec{v}\cdot\vec{x}}{}_1F_1(-i\nu_T, 1, -ivx-i\vec{v}\cdot\vec{x})$ is the electronic continuum Coulomb wave function in the attractive electrostatic field $V_T=-Z_T^{\rm eff}/x$. Therefore, the combined modifying function (for the nucleus-nucleus and nucleus-electron degrees of freedom) of the final unperturbed state Φ_f is the product $D_f(\vec{R})d_f(\vec{x})$. The electronic plane wave $e^{i\vec{v}\cdot\vec{x}}$ from the Coulomb wave $\varphi_{\vec{v}}^-(\vec{x})$ is incorporated into the term $e^{-i\vec{k}_f\cdot\vec{r}_f}$ from Φ_f. It is for this reason that $e^{i\vec{v}\cdot\vec{x}}$ is absent from $d_f(\vec{x})$ which, therefore, appears in (2) as the reduced Coulomb continuum wave function $d_f(\vec{x})=N^-(\nu_T){}_1F_1(-i\nu_T, 1, -ivx-i\vec{v}\cdot\vec{x})$.

Finally, capture of the electron occurs from this latter intermediate ionizing state (capture from continuum), because the electron e travels with the velocity vector $\vec{v}$ as does the scattered projectile P of charge Z_P. As a consequence, the attractive Coulomb potential between Z_P and e is sufficient to bind them together into the newly formed hydrogen-like atomic system $(Z_P, e)_f$.

Returning to (2), the last line therein follows from: $\exp[(i/v)Z_P(Z_T^{\rm eff}-1)\ln(vR-\vec{v}\cdot\vec{R})]\ \{\exp[-(i/v)Z_PZ_T^{\rm eff}\ln(vR+\vec{v}\cdot\vec{R})]\}^*=(\rho v)^{2iZ_P(Z_T^{\rm eff}-1)/v}(vR+\vec{v}\cdot\vec{R})^{i\xi}$ where $\xi=Z_P/v$ as in (2). Since $(\rho v)^{2iZ_P(Z_T^{\rm eff}-1)/v}$ does not contribute to the total cross section Q_{if} [8], it can be dropped from (2). Thus, concerning Q_{if}, it is merely the phase $(vR+\vec{v}\cdot\vec{R})^{i\xi}$ which remains in (2) from the overall modifying factor $D_i(\vec{R})D_f^*(\vec{R})$ of the relative motion of the heavy scattering aggregates.

Regarding the confluent hypergeometric function ${}_1F_1(i\nu_T, 1, ivx+i\vec{v}\cdot\vec{x})$ from equation (2), the following integral representation is useful:

$$ {}_1F_1(i\nu_T, 1, ivx+i\vec{v}\cdot\vec{x})=\frac{1}{\Gamma(i\nu_T)\Gamma(1-i\nu_T)}\times\int_0^1 d\tau\tau^{i\nu_T-1}(1-\tau)^{-i\nu_T}e^{i(vx+\vec{v}\cdot\vec{x})\tau}, \tag{3}$$

where an infinitesimally small negative imaginary part $-i\epsilon\,(\epsilon>0)$ is assumed to be implicitly added to the parameter ν_T via $\nu_T\to\nu_T-i\epsilon$ in order to secure convergence of the integral. Upon carrying out the calculation, the limit $\epsilon\to0^+$ is taken, where the plus superscript indicates that ϵ tends to zero through positive numbers. Then, for the purpose of Q_{if}, we can ignore the nucleus-nucleus term $(\rho v)^{2iZ_P(Z_T^{\rm eff}-1)/v}$ in (2) so that:

$$ T_{if}(\vec{\eta})=\mathcal{M}\int_0^1 d\tau\tau^{i\nu_T-1}(1-\tau)^{-i\nu_T}\mathcal{S}_{if}(\tau),\quad \mathcal{M}=[N^-(\nu_T)]^*/[\Gamma(i\nu_T)\Gamma(1-i\nu_T)], \tag{4}$$

$$ \mathcal{S}_{if}(\tau)=\int d\vec{R}e^{i\vec{\beta}\cdot\vec{R}}(vR+\vec{v}\cdot\vec{R})^{i\xi}\mathcal{T}(\vec{R}), \tag{5}$$

$$ \mathcal{T}(\vec{R})=Z_P\int d\vec{s}\,\varphi_f^*(\vec{s}\,)\varphi_i(\vec{x})\left(\frac{1}{R}-\frac{1}{s}\right)e^{-i\vec{v}\cdot\vec{s}+i(vx+\vec{v}\cdot\vec{x})\tau}. \tag{6}$$

Using [56–59], we made two choices of the target initial ground-state RHF wave function $\varphi_i(\vec{x})$ as the fixed linear combinations of normalized STOs. Presently, the calculation of total cross sections will be performed for single electron capture separately from the K- and L-shells of a lithium atom by protons and alpha particles. For the other atomic targets (carbon, nitrogen, oxygen and neon), only capture from their K-shells will be taken into account. For all these targets, the wave function $\varphi_i(\vec{x})$ reads as [56]:

Table 1. Expansion coefficients for orbitals and the RHF orbital energies of the target atoms. Notation $\pm 1.2345, -n$ implies $\pm 1.2345 \times 10^{-n}$.

	Li(^{2}S), φ_{1s}	Li(^{2}S), φ_{2s}	C(^{3}P), φ_{1s}	N(^{4}S), φ_{1s}	O(^{3}P), φ_{1s}	Ne(^{1}S), φ_{1s}
c_1	3.499 67	−0.57021	11.820 14	15.388 48	19.858 01	27.375 67
c_2	1.133 72	−0.15441	2.023 88	2.184 13	1.730 34	3.008 63
N_1	−4.20671,−6	1.982 41,−4	5.510 72,−4	1.166 80,−3	−7.37761,−4	1.805 20,−3
N_2	2.293 09,−4	2.007 54	−2.91479,−3	−4.86689,−3	1.347 98,−2	−5.13026,−3
N_3	−1.47690,−3	7.501 45,−2	3.810 21,−2	6.324 58,−2	−1.08333,−1	1.627 05,−1
N_4	1.736 57,−2	−2.16501	7.977 63,−2	3.217 50	1.771 14	1.956 29
E_i^{RHF}	−2.47773	−0.19632	−11.32554	−15.62909	−20.66866	−32.77248

Table 2. Damping factors in the exponentials of the orbitals in the target atoms.

	Li(^{2}S), φ_{1s}	Li(^{2}S), φ_{2s}	C(^{3}P), φ_{1s}	N(^{4}S), φ_{1s}	O(^{3}P), φ_{1s}	Ne(^{1}S), φ_{1s}
ζ_1	2.476 73	2.476 73	5.435 99	6.457 39	7.614 13	9.484 86
ζ_2	4.698 73	4.698 73	9.482 56	11.172 00	13.757 40	15.565 90
λ_1	0.383 50	0.383 50	1.057 49	1.364 05	1.698 24	1.961 84
λ_2	0.660 55	0.660 55	1.524 27	1.897 34	2.480 22	2.864 23
λ_3	1.070 00	1.070 00	2.684 35	3.252 91	4.311 96	4.825 30
λ_4	1.632 00	1.632 00	4.200 96	5.082 38	5.865 96	7.792 42

$$\varphi_i(\vec{x}) \equiv \varphi_{nlm}^{\mathrm{RHF}}(\vec{x}) = \frac{1}{\sqrt{\pi}} \sum_{i=1}^{i_{\max}} c_i \mathrm{e}^{-\zeta_i x} + \frac{1}{\sqrt{\pi}} \sum_{j=1}^{j_{\max}} N_j x \mathrm{e}^{-\lambda_j x}, \tag{7}$$

where the values of the parameters c_i, N_j, ζ_i, λ_j and E_i^{RHF} from [56] are summarized in tables 1 and 2. Here, $i_{\max}$ and $j_{\max}$ denote the numbers of the $1s$ and $2s$ STOs, respectively, in the RHF wave functions (presently $i_{\max} = 2$ and $j_{\max} = 4$).

The following hydrogenic relation will be used for the effective charge $Z_{\mathrm{T}}^{\mathrm{eff}}$, as suggested in [8]:

$$Z_{\mathrm{T}}^{\mathrm{eff}} = n\sqrt{-2E_i^{\mathrm{RHF}}}, \tag{8}$$

where n is the principal quantum number of the target initial orbital from which the active electron is transferred to the projectile.

Employing equation (7) and the hydrogen-like wave function for the ground-state $\varphi_f(\vec{s}) = \sqrt{Z_{\mathrm{P}}^3/\pi}\,\mathrm{e}^{-Z_{\mathrm{P}}s}$, the quantity $\mathcal{T}(\vec{R})$ from equation (6) becomes:

$$\mathcal{T}(\vec{R}) = Z_{\mathrm{P}}\left[\frac{1}{R}(W_{R1} + W_{R2}) - (W_{s1} + W_{s2})\right], \tag{9}$$

where

$$W_{R1} = \frac{Z_{\mathrm{P}}^{3/2}}{\pi} \sum_{i=1}^{i_{\max}} c_i \int \mathrm{d}\vec{s}\ \mathrm{e}^{-i\vec{v}\cdot\vec{s} - Z_{\mathrm{P}}s}[\mathrm{e}^{-\zeta_i x + i(vx + \vec{v}\cdot\vec{x})\tau}], \tag{10}$$

$$W_{R2} = \frac{Z_{\mathrm{P}}^{3/2}}{\pi} \sum_{j=1}^{j_{\max}} N_j \int \mathrm{d}\vec{s}\ \mathrm{e}^{-i\vec{v}\cdot\vec{s} - Z_{\mathrm{P}}s}[x\mathrm{e}^{-\lambda_j x + i(vx + \vec{v}\cdot\vec{x})\tau}], \tag{11}$$

$$W_{s1} = \frac{Z_{\mathrm{P}}^{3/2}}{\pi} \sum_{i=1}^{i_{\max}} c_i \int \mathrm{d}\vec{s}\ \frac{\mathrm{e}^{-i\vec{v}\cdot\vec{s} - Z_{\mathrm{P}}s}}{s}[\mathrm{e}^{-\zeta_i x + i(vx + \vec{v}\cdot\vec{x})\tau}], \tag{12}$$

$$W_{s2} = \frac{Z_{\mathrm{P}}^{3/2}}{\pi} \sum_{j=1}^{j_{\max}} N_j \int \mathrm{d}\vec{s}\ \frac{\mathrm{e}^{-i\vec{v}\cdot\vec{s} - Z_{\mathrm{P}}s}}{s}[x\mathrm{e}^{-\lambda_j x + i(vx + \vec{v}\cdot\vec{x})\tau}]. \tag{13}$$

For the analytical part of our calculation, we will utilize the following Fourier transforms:

$$\mathrm{e}^{-\zeta_i x + i(vx + \vec{v}\cdot\vec{x})\tau} = \frac{\mu_i}{\pi^2} \int \mathrm{d}\vec{q} \frac{\mathrm{e}^{-i\vec{q}\cdot\vec{x}}}{(q_1^2 + \mu_i^2)^2}, \tag{14}$$

$$x\mathrm{e}^{-\lambda_j x + i(vx + \vec{v}\cdot\vec{x})\tau} = \frac{1}{\pi^2} \int \mathrm{d}\vec{q}\,\mathrm{e}^{-i\vec{q}\cdot\vec{x}} \times \left[\frac{4\mu_j^2}{(q_1^2 + \mu_j^2)^3} - \frac{1}{(q_1^2 + \mu_j^2)^2}\right], \tag{15}$$

where $\vec{q}_1 = \vec{q} + \vec{v}\tau$, $\mu_i = \zeta_i - iv\tau$ and $\mu_j = \lambda_j - iv\tau$. Also needed is the Feynman parametrization integral:

$$\frac{1}{A^s B^r} = \frac{(s + r - 1)!}{(s - 1)!(r - 1)!} \times \int_0^1 \mathrm{d}t \frac{t^{s-1}(1 - t)^{r-1}}{[At + B(1 - t)]^{s+r}} \qquad (s, r \geqslant 1). \tag{16}$$

These preliminaries enable an analytical reduction of the quantities W_{R1}, W_{R2}, W_{s1} and W_{s2} to the following one-dimensional integrals over a real variable t:

$$W_{R1} = 2Z_{\mathrm{P}}^{5/2}\mathrm{e}^{-i\vec{\beta}\cdot\vec{R}} \int_0^1 \mathrm{d}t\, t(1 - t) \times \sum_{i=1}^{i_{\max}} \frac{c_i \mu_i}{\Delta_i^5}(3 + 3\Delta_i R + \Delta_i^2 R^2)\mathrm{e}^{-i\vec{Q}_1\cdot\vec{R} - \Delta_i R}, \tag{17}$$

$$W_{R2} = 2Z_P^{5/2} e^{-i\vec{\beta}\cdot\vec{R}} \int_0^1 dt t(1-t) \sum_{j=1}^{j_{max}} \frac{N_j}{\Delta_j^5} [3(5p_j - 1) + 3\Delta_j(5p_j - 1)R + \Delta_j^2(6p_j - 1)R^2 + \Delta_j^3 p_j R^3] e^{-i\vec{Q}_1\cdot\vec{R} - \Delta_j R}, \quad (18)$$

$$W_{s1} = 2Z_P^{3/2} e^{-i\vec{\beta}\cdot\vec{R}} \int_0^1 dt(1-t) \times \sum_{i=1}^{i_{max}} \frac{c_i \mu_i}{\Delta_i^3} (1 + \Delta_i R) e^{-i\vec{Q}_1\cdot\vec{R} - \Delta_i R}, \quad (19)$$

$$W_{s2} = 2Z_P^{3/2} e^{-i\vec{\beta}\cdot\vec{R}} \int_0^1 dt(1-t) \sum_{j=1}^{j_{max}} \frac{N_j}{\Delta_j^3} [(3p_j - 1) + \Delta_j(3p_j - 1)R + \Delta_j^2 p_j R^2] e^{-i\vec{Q}_1\cdot\vec{R} - \Delta_j R}, \quad (20)$$

where $\Delta_k^2 = v_1^2 t(1-t) + Z_P^2 t + \mu_k^2 (1-t)$, $(k = i, j)$, $\vec{v}_1 = \vec{v}(1-\tau)$, $p_j = \mu_j^2(1-t)/\Delta_j^2$, $\vec{Q}_1 = -(\vec{v} + \vec{\beta})t - \vec{\beta}_1(1-t)$ and $\vec{\beta}_1 = \vec{\beta} + \vec{v}\tau$.

With the help of the results from (17)–(20) and by employing (9), the quantity $\mathcal{S}_{if}(\tau)$ from (5) can be expressed in terms of the typical integral:

$$I_n = \int d\vec{R} R^{n-1} e^{-i\vec{Q}_1\cdot\vec{R} - \Delta_k R} (vR + \vec{v}\cdot\vec{R})^{i\xi}. \quad (21)$$

Making use of the analytical results for $I_n (n = 0, 1, 2, 3)$ from [20], we arrived at the final expression for the transition amplitude T_{if} which is given by this two-dimensional integral over the real variables t and τ:

$$T_{if}(\vec{\eta}) = \mathcal{K} \int_0^1 d\tau f(\tau) \int_0^1 dt(1-t) \times \left[\sum_{i=1}^{i_{max}} \frac{c_i \mu_i}{\Delta_i^3} (\nu_i - i\xi\delta_i) + \sum_{j=1}^{j_{max}} \frac{N_j}{\Delta_j^3} (\nu_j - i\xi\delta_j) \right], \quad (22)$$

where $\mathcal{K} = 8\pi Z_P^{5/2} \Gamma(1 + i\xi)\mathcal{M}$ and $f(\tau) = \tau^{i\nu_T - 1}(1-\tau)^{-i\nu_T}$. The expressions for the quantities ν_i, ν_j, δ_i and δ_j are listed in the Appendix. The remaining two-dimensional integral in (22) is computed numerically to obtain the transition amplitude $T_{if}(\vec{\eta})$ from (4).

Then with the $T-$matrix element (22) at hand, the total cross section denoted by Q_{if} is represented by this formula:

$$Q_{if}(\pi a_0^2) = \frac{1}{2\pi^2 v^2} \int_0^\infty d\eta \eta |T_{if}(\vec{\eta})|^2. \quad (23)$$

As such, the total cross section in the BCIS method is generated by way of three numerical integrations (over τ, t and η) for which we employ the Gauss-Legendre quadrature. Before performing these numerical integrations, the Cauchy regularization [19] is used for the $\tau-$quadrature to avoid the double singularity of the function $f(\tau)$ at $\tau = 0$ and $\tau = 1$ arising from the representation (3) of the hypergeometric function. Also, an appropriate change of variable [15] is made in the $\eta-$integration according to $z = (\eta^2 - 2)/(\eta^2 + 2)$ which scales the integrand toward the dominant region of the narrow forward cone of scattering (appropriate for heavy particle collisions within the eikonal approximation [8]).

The explicit computations are carried out only for the initial and final ground states. The obtained theoretical results are multiplied by a factor of 1.202 which is an approximate contribution (~20%) from all the excited states according to the n_f^{-3} Oppenheimer scaling law. At every impact energy for all the considered processes, a total of 368 integration points was used for each of the three quadratures. Convergence rate as a function of the number of the integration points is also examined.

3. Results and discussion

Here, we shall present the new cross sections obtained by means of the BCIS method within the RHF model. Specifically, we consider the following scattering processes:

$$H^+ + \begin{cases} Li(1s^2 2s^1) \\ Li(1s^2 2s^1) \end{cases} \longrightarrow H(1s) + \begin{cases} Li^+(1s^1 2s^1), \text{ after the K} - \text{shell capture} \\ Li^+(1s^2), \text{ after the L} - \text{shell capture} \end{cases}, \quad (24)$$

$$He^{2+} + \begin{cases} Li(1s^2 2s^1) \\ Li(1s^2 2s^1) \end{cases} \longrightarrow He^+(1s) + \begin{cases} Li^+(1s^1 2s^1), \text{ after the K} - \text{shell capture} \\ Li^+(1s^2), \text{ after the L} - \text{shell capture} \end{cases}, \quad (25)$$

$$H^+ + \begin{cases} C(1s^2 2s^2 2p^2) \\ N(1s^2 2s^2 2p^3) \\ O(1s^2 2s^2 2p^4) \\ Ne(1s^2 2s^2 2p^6) \end{cases} \longrightarrow H(1s) + \begin{cases} C^+(1s^1 2s^2 2p^2) \\ N^+(1s^1 2s^2 2p^3) \\ O^+(1s^1 2s^2 2p^4) \\ Ne^+(1s^1 2s^2 2p^6) \end{cases}, \quad (26)$$

$$He^{2+} + \begin{cases} C(1s^2 2s^2 2p^2) \\ Ne(1s^2 2s^2 2p^6) \end{cases} \longrightarrow He^+(1s) + \begin{cases} C^+(1s^1 2s^2 2p^2) \\ Ne^+(1s^1 2s^2 2p^6) \end{cases}. \quad (27)$$

In the present computations, we have not accounted for the final states of the target ion after collision. As mentioned, these disappear altogether from the T-matrix elements on account on the independent particle formalism, the frozen-core approximation and the fact that only one electron is taken as active. The configurations in the exit channels from (26) and (27) are written only to indicate the K-shell capture $1s^2 \rightarrow 1s$.

First, we shall consider the $H^+ + Li$ and $He^{2+} + Li$ collisions for which the obtained results are displayed in figures 1 and 2. For a lithium target atom, when the separately computed cross sections Q^K and Q^L for capture from the K- and L-shell, respectively, are added the result is denoted by Q^{K+L} i.e. $Q^{K+L} = Q^K + Q^L$ where, for brevity, $Q_{if} \equiv Q$. Moreover, the cross sections for capture from the K-shell are multiplied by 2 because each of the two electrons from this shell can be captured with equal probabilities. No such a multiplication is made for capture for the L-shell which has only one electron in a lithium atom.

As can be seen from figures 1 and 2, at lower impact energies, the total capture cross sections are dominated by capture from the L-shell of Li. However, when the projectile energy increases, capture from the K-shell begins to play the

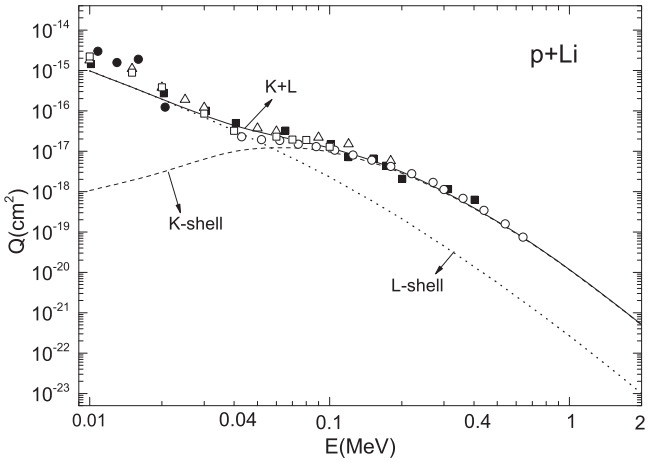

Figure 1. Total cross sections $Q_{if} \equiv Q$ (in cm^2) for one electron capture from all the shells of lithium by protons: $H^+ + Li \longrightarrow H + Li^+$. The dashed, dotted and full curves are the present results for the total cross sections Q^K, Q^L and Q^{K+L} in the prior version of the BCIS method within the RHF model [56] for electron capture from the K-, L- and (K + L)-shells of Li, respectively. Experimental data: △ Il'in *et al* [60], □ DuBois and Toburen [61], ∘ Shah *et al* [62], • Grüebler *et al* [63], ■ D'yachkov [64].

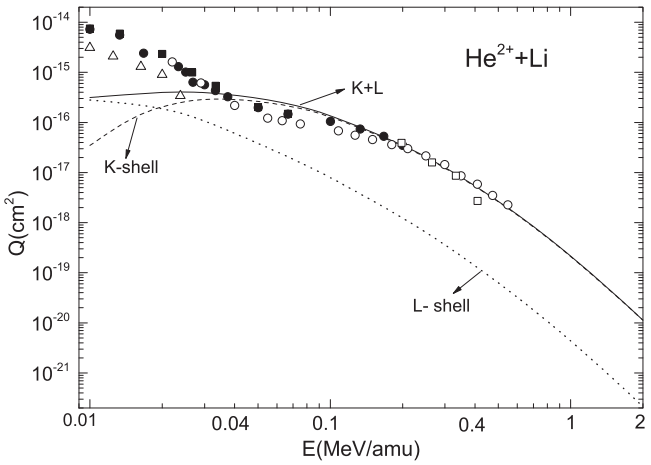

Figure 2. Total cross sections $Q_{if} \equiv Q$ (in cm^2) for one electron capture from all the shells of lithium by alpha particles: $He^{2+} + Li \longrightarrow He^+ + Li^+$. The dashed, dotted and full curves are the present results for the total cross sections Q^K, Q^L and Q^{K+L} in the prior version of the BCIS method within the RHF model [56] for electron capture from the K-, L- and (K + L)-shells of Li, respectively. Experimental data: ■ DuBois and Toburen [61], ∘ Shah *et al* [62], □ Sassao *et al* [65], • McCullough *et al* [66], △ Murray *et al* [67].

dominant role. The cross sections for capture from the K-shell in the $H^+ + Li$ collisions are found in figure 1 to be relatively small for energies lower than 50 keV. In general, the contribution for the L-shell electron capture increases with decreased projectile energy. A comparison for capture from any shell (full curve) with a number of measurements [60–64] shows excellent agreement throughout the considered impact energy range.

The total cross sections Q^K, Q^L and Q^{K+L} in in the BCIS method for single electron capture by He^{2+} from the L-, K- and (K+L)-shells of Li(^{2}S), computed in a wide range of energies between 10 keV/amu and 2 MeV/amu, are

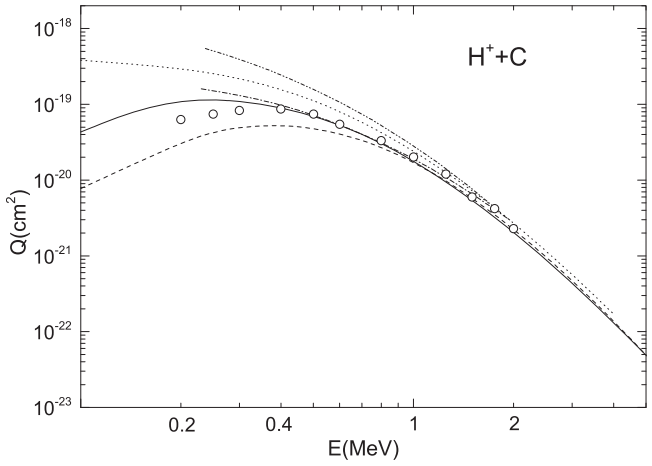

Figure 3. The K-shell electron capture cross sections (in cm^2) as a function of the laboratory incident energy E(MeV) for the collisional process: $H^+ + C \longrightarrow H + C^+$. The full curve is for the present results in the BCIS method within the RHF model [56] for one electron capture from the K-shell. The dashed curve represents the cross sections in the BCIS method with the hydrogen-like wave function for the target [46]. The dotted curve represents the cross sections from the CB1 method [18]. The dash-dotted and dash-double dotted curves are cross sections from the prior and post version of the CBDW method [23], respectively. Experimental data: ∘ Rødbro *et al* [68].

displayed in figure 2. Therein, it can be seen that, above 30 keV/amu, the cross sections Q^{K+L} for electron capture from any shell, i.e. from the (K+L)-shell, are in very good agreement with the experimental data from [61, 62, 65–67]. At lower impact energies, the theoretical curve lies below the data from the measurements. This situation would be improved by an explicit inclusion of the contribution from capture into the excited states (i.e. not roughly through the Oppenheimer scaling rule n_f^{-3} as done presently).

The cross sections shown in figure 3 for single electron capture by protons from the K-shell of C(^{3}P) are computed for a range of impact energies between 100 keV and 5 MeV. Herein, the two versions of the BCIS method are presented, depending on the wave function used for the ground-state of the target (one with the hydrogen-like and the other with the RHF wave function). The effective nuclear charge $Z_T^{\rm eff}$ is used in both the hydrogen-like wave function, $\varphi_i(\vec{x}) = [(Z_T^{\rm eff})^{3/2}/\sqrt{\pi}\,]e^{-Z_T^{\rm eff}x}$, and the associated eigen-energy, $E_i = -(Z_T^{\rm eff})^2/2$. For the hydrogenic model, $Z_T^{\rm eff}$ is taken to be the screened target nuclear charge, $Z_T^{\rm eff} = Z_T - 5/16$, where 5/16 is the Slater screening factor.

For comparisons with the present results, figure 3 also displays the cross sections from the CB1 method [18] (dotted curve) as well as from the two versions of the three-body Coulomb-Born distorted wave (CBDW) method [23]: prior (dash-dotted curve) and post (dash-double dotted curve). In [23], the single-zeta wave function [56] has been used to describe the initial target wave function of the active electron. On the other hand, in [18] the RHF wave function [56] has been utilized. It is clear from figure 3 that the prior cross sections are lower than their post counterparts from the CBDW method. In [18], the

post-prior discrepancy has been avoided by the introduction of the average T-matrix, $T_{if} = (T_{if}^{-} + T_{if}^{+})/2$. The ensuing averaged cross sections from the CB1 method are depicted in figure 3. As can be seen in figure 3, the two versions of the CBDW method and the averaged cross sections from the CB1 method overestimate both the results from the BCIS method and the experimental data, especially at lower impact energies.

It should be noted, that the CBDW and CB1 methods obey the correct boundary conditions. However, there are two main differences between these two methods. One is that the former and the latter employ the full Coulomb wave functions and the corresponding Coulomb logarithmic phases, respectively, for the relative motion of heavy particles. The other difference is that the CB1 method uses the forward-angle simplification, whereas the CBDW method does not. In other words, the CB1 method is the eikonal version of the CBDW method. Otherwise, the CBDW and CB1 methods have the same perturbation potential in the prior and post forms of the transition amplitudes. For the same initial target wave function, the use of either the full Coulomb wave function for the relative motion of heavy nuclei or its Coulomb logarithmic phase should give the same total cross sections in the CBDW and CB1 methods. The differences seen in figure 3 between the CBDW and CB1 methods should be due only to the use of two different initial target wave functions: the single-zeta and the RHF functions, respectively.

On a wide interval of impact energies, the results from the BCIS method within the RHF model [56] for electron capture by protons from the K-shell of nitrogen N(^{4}S) and oxygen O(^{3}P) are seen in figures 4 and 5, respectively, to be in good agreement with the experimental data from [69–77]. Herein, only the measurements of Cocke *et al* [69] correspond to capture from the K-shell of the target. All the other measured data displayed in figures 4 and 5 are for capture from any shell of nitrogen and oxygen. Moreover, here and throughout this study, the theory is for atomic targets, whereas all the experimental results shown in figures 4 and 5 are for molecular targets (N_2 and O_2). However, at high energies, the K-shell cross sections for these molecular targets can be converted to the atomic targets N and O by means of the scaling rule $Q_N = Q_{N_2}/2$ and $Q_O = Q_{O_2}/2$. As in figure 3, also shown in figures 4 and 5 are the cross sections from the CB1 method [15] as well as from the post and prior versions of the CBDW method [23].

The cross sections for formation of the atomic hydrogen in the $H^+ + Ne(^1S)$ collisions (proton-neon) are shown in figure 6 alongside the experimental data [68, 69]. The present results obtained with the RHF wave function [56] for the target ground state are observed to overestimate the measured data at lower energies. However, at higher impact energies (above 2 MeV), very good agreement is seen between our findings and the measurements. The cross sections from the CDW method [8] with the RHF wave function [56] and from the prior version of the CBDW method [23] with single zeta function [56] are also given in figure 6 by the dash-dotted and dotted curves, respectively.

For electron capture by alpha particles from the K-shell of carbon C(^{3}P) and neon Ne(^{1}S), the theories and measurements are compared in figures 7 and 8, respectively. Within the BCIS method, there is significant discrepancy at lower

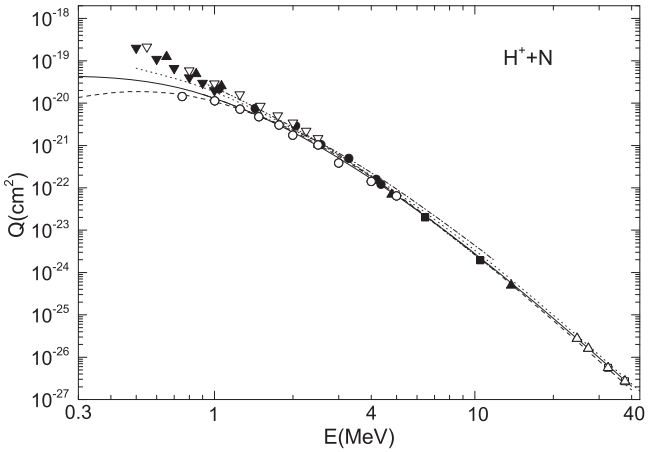

Figure 4. The same as in figure 3, except for the process $H^+ + N \longrightarrow H + N^+$ and for a different set of measurements. Experimental data: ∘ Cocke *et al* [69], □ Acerbi *et al* [70], △ Acerbi *et al* [71], • Schryber *et al* [72], ▲ Welsh *et al* [73], ▽ Toburen *et al* [74], ■ Berkner *et al* [75], ▼ Allison *et al* [76].

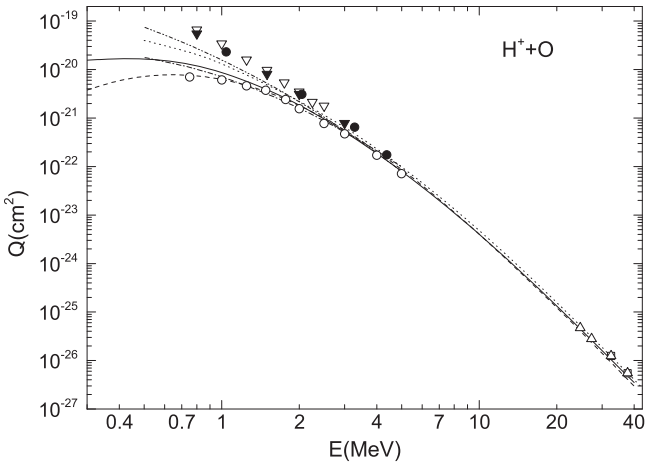

Figure 5. The same as in figure 3, except for the process $H^+ + O \longrightarrow H + O^+$ and for a different set of measurements. Experimental data: ∘ Cocke *et al* [69], □ Acerbi *et al* [70], △ Acerbi *et al* [71], • Schryber *et al* [72], ▽ Toburen *et al* [74], ▼ Varghese *et al* [77].

impact energies between the results obtained by using the RHF [56] and the hydrogen-like wave functions. A satisfactory agreement is obtained for the $He^{2+} + C$ collisions between the BCIS with the RHF function [56] and the experimental data. As to the $He^{2+} + Ne$ collisions, throughout the entirely impact energy range from 300 keV/amu to 30.5 MeV/amu, the measured cross sections [68, 78] are excellently reproduced by the BCIS method with the RHF wave function [56]. Moreover, the maximum in figure 8 predicted by the BCIS method with the RHF function [56] occurs at the same energy as in the experimental data from [68]. As can be seen from figures 7 and 8, the results of the CDW method [8] (dash-dotted curve) overestimate those due to the BCIS method and measurements.

The results from the BCIS method with the hydrogen-like wave function [46] are shown by the dashed curves in

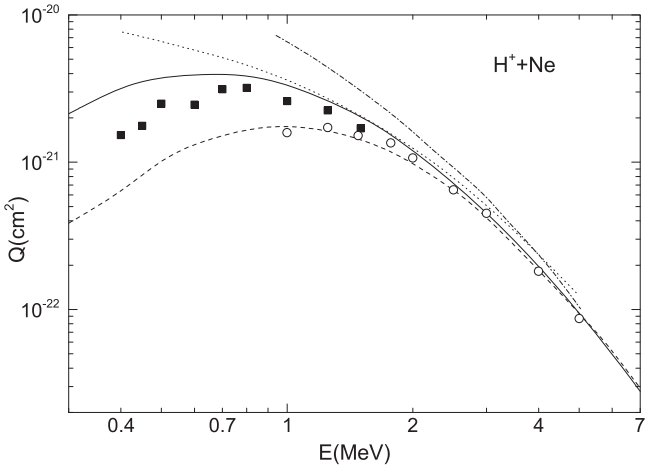

Figure 6. The K-shell electron capture cross sections (in cm^2) as a function of the laboratory incident energy E(MeV) for the collisional process: $H^+ + Ne \longrightarrow H + Ne^+$. The full curve is for the present results in the BCIS method within the RHF model [56] for one electron capture from the K-shell. The dashed curve represents the cross sections in the BCIS method with the hydrogen-like wave function for the target [46]. The dotted curve represents the cross sections from the prior version of the CBDW method [23]. The dash-dotted curve is for the cross sections in the CDW method [8]. Experimental data: ■ Rødbro *et al* [68], ∘ Cocke *et al* [69].

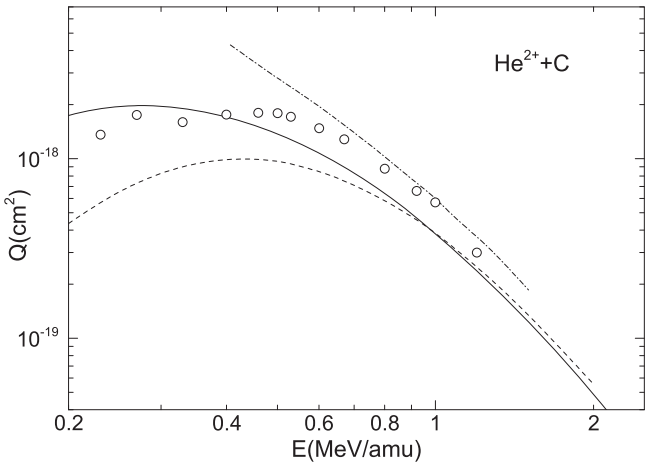

Figure 7. The same as in figure 6, except for the process $He^{2+} + C \longrightarrow He^+ + C^+$ and for a different set of measurements. Experimental data: ∘ Rødbro *et al* [68].

figures 3–8. At higher energies, both curves (full and dash) from the BCIS method are very near each other and, moreover, they closely follow the trend of the experimental data. However at lower energies, these theoretical curves display quite different behaviors. Namely, the results within the RHF model [56] overestimate those from the usage of the hydrogen-like wave function. In general, however, as can be seen from figures 3–8, the results from the BCIS method with the RHF wave function [56] are in better agreement with experimental data than the findings with the hydrogen-like wave function.

The main reason for the discrepancies between the cross sections from the BCIS method with the hydrogen-like (HYD) and the RHF wave functions [56] lies in very different

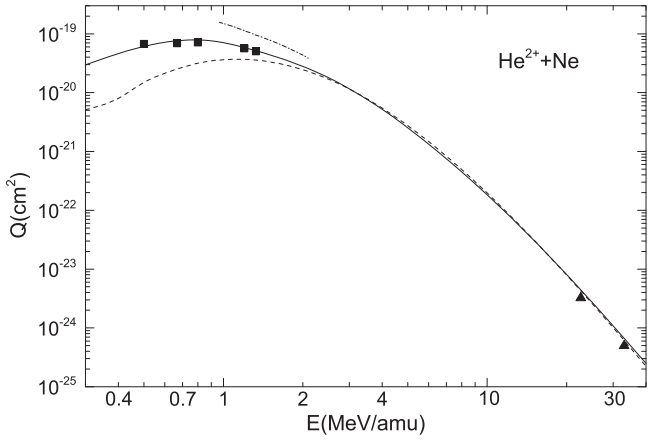

Figure 8. The same as in figure 6, except for the process $He^{2+} + Ne \longrightarrow He^+ + Ne^+$ and for a different set of measurements. Experimental data: ■ Rødbro *et al* [68], ▲ Katayama *et al* [78].

binding energies and the associated effective charges. For example, in the case of carbon atom, within the HYD model, the binding energy and the associated effective charge are $E_i^{\mathrm{HYD}} = -16.173828$ and $Z_{\mathrm{HYD}}^{\mathrm{eff}} = 5.6875$. In this case, the corresponding values from the RHF model [56] are $E_i^{\mathrm{RHF}} = -11.32554$ and $Z_{\mathrm{RHF}}^{\mathrm{eff}} = 4.7593$. From the nature of electron capture, it is expected that the effective charge should be strongly influential through the Sommerfeld parameter $\nu_{\mathrm{T}} = Z^{\mathrm{eff}}/v$ in the Coulomb wave function for the continuum intermediate states in the transition amplitude (2). The related question is: how much influence could be attributed to the two different forms of the target wave functions (the hydrogen-like versus the RHF) for the same discussed target parameters. To examine this feature, we used the BCIS method to perform a numerical experiment for electron capture from the K-shell of the carbon ground state in the $H^+ + C$ collisions. Namely, we employed the RHF wave function with the expansion coefficients and the exponential damping factors from [56], but with the HYD binding energy $E_i^{\mathrm{HYD}} = -16.173828$ instead of the RHF value $E_i^{\mathrm{RHF}} = -11.32554$. Moreover, within this setting, in the Sommerfeld parameter $\nu_{\mathrm{T}} = Z_{\mathrm{T}}^{\mathrm{eff}}/v$, entering the continuum Coulomb wave function, the RHF effective target nuclear charge $Z_{\mathrm{RHF}}^{\mathrm{eff}} = 4.7593$ is replaced by its HYD counterpart $Z_{\mathrm{HYD}}^{\mathrm{eff}} = 5.6875$. For this auxiliary model, provisionally called the RHF-HYD model, the obtained total cross sections for all the impact energies (100—5000 keV) were very close to those with the purely HYD model. Hence, as opposed to the target binding energy and effective charge, the specific form of the target wave function is inconsequential.

In order to investigate the sensitivity of the total cross sections to the choice of the target basis set, we employ two different RHF wave functions: the RHF1 [56] and the RHF2 [57–59]. Thus far and throughout, whenever the acronym RHF is used, it is by default referred to the RHF1 model [56]. The parameters of the RHF1 wave function are given in tables 1 and 2. On the other hand, for the ground state of carbon, $C(^3P)$, the RHF2 wave function has five $1s$ and three $2s$ normalized STOs with the parameters: $c_1 = -6.29084$, $\zeta_1 = 9.23879$,

Table 3. The present total cross sections (in cm^2) in the prior version of the BCIS method for electron capture from the target K-shells in the $H^+ + C$ and $He^{2+} + Ne$ collisions for different ground-state wave functions: the single-zeta function, SZF [56]; the double-zeta function, DZF [56]; the RHF1 [56], RHF2 [57–59].

$H^+ + C$ collision				
E(MeV)	SZF	DZF	RHF1	RHF2
0.1	4.5310,−20	4.3135,−20	4.3343,−20	4.3328,−20
0.15	8.7174,−20	8.7117,−20	8.7020,−20	8.7022,−20
0.2	1.1083,−19	1.1363,−19	1.1321,−19	1.1323,−19
0.3	1.1388,−19	1.1770,−19	1.1748,−19	1.1747,−19
0.5	7.3225,−20	7.4527,−20	7.4401,−20	7.4396,−20
0.75	3.4883,−20	3.6139,−20	3.6095,−20	3.6091,−20
1	1.7803,−20	1.8246,−20	1.8197,−20	1.8199,−20
1.5	5.6545,−21	5.5697,−21	5.5817,−21	5.5816,−21
2	2.1699,−21	2.0852,−21	2.0982,−21	2.0975,−21
3	4.6590,−22	4.4025,−22	4.4317,−22	4.4318,−22
4	1.3869,−22	1.3143,−22	1.3180,−22	1.3187,−22
5	5.1010,−23	4.8813,−23	4.8753,−23	4.8784,−23
$He^{2+} + Ne$ collision				
E(MeV/amu)	SZF	DZF	RHF1	RHF2
0.3	3.1073,−20	2.9698,−20	2.9756,−20	2.9750,−20
0.5	6.6168,−20	6.6309,−20	6.6252,−20	6.6259,−20
0.75	8.0571,−20	8.2230,−20	8.2391,−20	8.2388,−20
1	7.4433,−20	7.5723,−20	7.5856,−20	7.5856,−20
2	2.9805,−20	2.9813,−20	3.0596,−20	3.0595,−20
3	1.1814,−20	1.1996,−20	1.1996,−20	1.1997,−20
4	5.3208,−21	5.2902,−21	5.2920,−21	5.2924,−21
5	2.6381,−21	2.5804,−21	2.5868,−21	2.5865,−21
7.5	6.1790,−22	5.9362,−22	5.9629,−22	5.9618,−22
10	1.9430,−22	1.8643,−22	1.8700,−22	1.8703,−22
15	3.2557,−23	3.1644,−23	3.1576,−23	3.1589,−23
20	8.3412,−24	8.2298,−24	8.1889,−24	8.1904,−24
30	1.0991,−24	1.1120,−24	1.1043,−24	1.1038,−24
40	2.4545,−25	2.5300,−25	2.5110,−25	2.5094,−25

$c_2 = -7.52355$, $\zeta_2 = 5.10037$, $c_3 = -2.41986 \times 10^{-2}$, $\zeta_3 = 3.27663$, $c_4 = -2.64897 \times 10^{-4}$, $\zeta_4 = 1.19296$, $c_5 = -5.91045 \times 10^{-5}$, $\zeta_5 = 0.93096$, $N_1 = -0.491606$, $\lambda_1 = 18.89045$, $N_2 = -13.04477$, $\lambda_2 = 7.51751$, $N_3 = -4.96865 \times 10^{-3}$, $\lambda_3 = 2.27024$ and the binding energy $E_i = -11.3255187$. As can be seen from table 3, the total cross sections computed with the RHF1 [56] and RHF2 [57–59] target wave functions are nearly the same.

Additionally, we used also the single-zeta wave function (SZF) with the parameters for $C(^3P)$ [56]: $c_1 = 13.47608$, $\zeta_1 = 5.67263$, $N_1 = 2.16483 \times 10^{-2}$, $\lambda_1 = 1.60833$ with $E_i = -11.30156$ and the double-zeta wave function (DZF) [56]: $c_1 = 4.77121$, $\zeta_1 = 7.52232$, $c_2 = 9.03253$, $\zeta_2 = 5.12306$, $N_1 = -9.13684 \times 10^{-3}$, $\lambda_1 = 1.83068$, $N_2 = 2.19142 \times 10^{-3}$, $\lambda_2 = 1.15282$ with $E_i = -11.32343$. The obtained results for total cross sections with the SZF and DZF are very close to those with the RHF1 [56] and RHF2 [57–59] target wave functions (see table 3).

Yet another illustration is reported in table 3 for a different collision system ($He^{2+} + Ne$) and for a wider impact energy interval. Here too, the obtained total cross sections with the SZF and DZF are nearly the same as those with the the RHF1 [56] and RHF2 [57–59]. Moreover, we verified that the same features also hold true for all the other collision systems investigated in the present work. It can then be safely concluded that the BCIS method is practically insensitive to the examined choices of the target ground-state wave functions.

Description of the *ground* state of the active electron in the multi-electron atomic targets under study (lithium, carbon, nitrogen, oxygen and neon) amounts to using different numbers of the $2s$ basis functions. Thus, for carbon atom, the four wave functions denoted by RHF1, RHF2, DZF and SZF contain four, three, two and one $2s-$basis functions, respectively. Since all the four wave functions give nearly the same results, it can be concluded that the actual number of the $2s$ basis orbitals does not impact noticeably on the values of the computed total cross sections.

As per the Theory Section, the three-body BCIS method used in this work accounts only for one active electron of a multi-electron target. All the other target electrons are considered as being passive (not participating to the capture probability of the active electron) within the accompanying frozen-core approximation. As such, the present version of

Table 4. The present total cross sections (in cm^2) in the prior version of the BCIS method for electron capture from the target K-shell for the $H^+ + O$ collisions as a function of the number of integration points used per each axis of the numerical quadrature for different incident proton energies. The initial ground-state (K-shell) of an oxygen atom is described by the RHF1 [56]. The first column denoted by NGL represents the number of integration points of the Gauss-Legendre quadrature. The notation e.g. 8.8902,−27 means 8.8902×10^{-27}.

NGL	300 keV	2000 keV	10 000 keV	40 000 keV
8	9.3494,−19	2.2015,−21	3.2019,−24	8.8902,−27
16	7.0508,−20	2.1625,−21	4.6702,−24	3.1019,−27
24	5.1647,−20	1.8212,−21	5.4976,−24	3.7035,−27
32	2.9848,−20	1.8957,−21	3.7785,−24	4.2000,−27
40	1.7645,−20	1.9068,−21	3.5385,−24	4.9320,−27
48	1.3011,−20	1.9000,−21	3.9826,−24	6.3040,−27
64	1.2722,−20	1.8974,−21	4.1716,−24	2.7268,−27
80	1.4628,−20	1.8969,−21	4.0251,−24	3.0885,−27
96	1.5871,−20	1.8970,−21	4.0985,−24	3.8573,−27
112	1.6385,−20	1.8972,−21	4.0664,−24	4.1701,−27
128	1.6473,−20	1.8975,−21	4.0783,−24	3.1924,−27
144	1.6368,−20	1.8977,−21	4.0741,−24	3.2460,−27
160	1.6198,−20	1.8979,−21	4.0753,−24	3.6415,−27
176	1.6026,−20	1.8980,−21	4.0749,−24	3.7203,−27
192	1.5879,−20	1.8982,−21	4.0749,−24	3.4081,−27
208	1.5764,−20	1.8983,−21	4.0749,−24	3.3761,−27
224	1.5679,−20	1.8983,−21	4.0749,−24	3.5406,−27
240	1.5622,−20	1.8984,−21	4.0748,−24	3.5790,−27
256	1.5586,−20	1.8985,−21	4.0748,−24	3.4707,−27
272	1.5566,−20	1.8985,−21	4.0748,−24	3.4473,−27
288	1.5558,−20	1.8986,−21	4.0748,−24	3.5083,−27
304	1.5559,−20	1.8986,−21	4.0748,−24	3.5267,−27
320	1.5565,−20	1.8986,−21	4.0748,−24	3.4888,−27
336	1.5575,−20	1.8986,−21	4.0748,−24	3.4771,−27
352	1.5587,−20	1.8987,−21	4.0748,−24	3.4991,−27
368	1.5601,−20	1.8987,−21	4.0748,−24	3.5071,−27
384	1.5615,−20	1.8987,−21	4.0748,−24	3.4938,−27
400	1.5628,−20	1.8987,−21	4.0748,−24	3.4887,−27

the BCIS method includes no correlation effects. To investigate these latter effects, the correlated wave functions (e.g. within the representation of configuration interactions) would be appropriate. However, this is outside of the scope of the present study, as it would necessitate a considerably more involved four-body version of the BCIS method for multi-electron targets.

Special attention has been paid to convergence during numerical integrations. In table 4, as an illustration, the results for the total cross sections for the $H^+ + O$ collisions are shown at four impact energies for different sets of the quadrature order NGL associated with some 8–400 integration points per each integration axis (NGL denotes the number of integration points of Gauss-Legendre quadrature). As expected, at lower impact energies fewer integration points are required to achieve good convergence. At the highest impact energies (40 MeV), cross sections as a function of NGL are seen in table 4 to slightly oscillate. This occurs because with a large increase in the incident velocity v, the Sommerfeld parameter $\nu_T = Z_T^{eff}/v$ becomes very small and this causes rapid oscillations of the function $f(\tau) = \tau^{i\nu_T - 1}(1 - \tau)^{-i\nu_T}$ from the integral representation of the hypergeometric function within the integral (22).

Note that, as usual, in the eikonal approximation adopted in the present work, all the computed cross sections should be given only with two decimal places. Tables 3 and 4 are an exception with four decimals that are quoted merely to monitor the convergence pattern with the increasing value of NGL.

4. Conclusions

Using the three-body boundary-corrected continuum intermediate state method, BCIS, we have investigated single electron capture from multi-electron atomic targets (lithium, carbon, nitrogen, oxygen and neon) colliding with fast protons and alpha projectiles. Within the independent particle model, the initial ground state of the captured electron is described by five analytical wave functions: the Roothan-Hartree-Fock, RHF, the single- and double-zeta and the hydrogen-like. Each wave function is used with its corresponding binding orbital energies of the active target electron. The captured electron is described in an asymmetric manner in the entrance and exit channels. Namely, the presently applied prior form of the BCIS method is a hybrid formalism, which is the combination of the continuum distorted wave method, CDW, in the exit channel and the boundary-corrected first Born method, CB1, in the entrance channel. The associated initial perturbation potential (the entrance channel) in the prior form of the transition amplitude coincides with the corresponding interaction encountered in the CB1 method.

The prior version of the BCIS method includes the continuum intermediate states of the captured electron in the exit channel through the use of the full Coulomb wave function centered on the screened target nucleus charge. There is no explicit purely electronic $\vec{s}-$ dependent Coulomb modifying factor in the entrance channel in the prior BCIS method. Such a factor (a Coulomb logarithmic phase) is included only asymptotically via its $\vec{R}-$ dependence in the overall compound aggregate-aggregate modifying term of the initial unperturbed state. Special attention is presently paid to the lithium target for which the cross sections are computed separately for single electron capture from the tightly bound K-shell and also from the loosely bound valence electron in the L-shell. For the other targets, the K-shell capture cross sections alone are reported. Detailed comparisons of the obtained results in the BCIS method with the available experimental data are made and overall good agreement is systematically recorded, particularly with the RHF wave functions.

The sensitivity of the computed total cross sections is thoroughly tested with respect to the mentioned five different target wave functions. The outcome is appealing: the total cross sections in the BCIS method are practically the same for four wave functions, the two analytical forms of the RHF functions and the two zeta functions. These results are also

similar to those from the hydrogen-like wave functions but only at sufficiently high impact energies with notable discrepancies occurring at intermediate energies. This latter discrepancy could, in principle, be due to different forms of the wave functions or to different binding energies (or both). To separate these two origins of the discrepancy, we performed a numerical experiment with a hybrid model (the RHF model plus the hydrogenic model). Namely, we used the form of the RHF wave function (with its expansions coefficients for the constituent Slater-type orbitals and the pertinent exponential damping factors), but with the binding energy of the hydrogen-like wave function (the latter energy is employed in the target nuclear effective charge). The resulting cross sections of this hybrid model are remarkable since they are nearly coincident with those of the purely hydrogen-like model. This clearly shows that the form of the target wave functions is not essential and that the principal origin of having different total cross sections in the RHF and hydrogenic models is due to the use of different target binding energies.

From the present results, it can be concluded that at intermediate and high impact energies, the BCIS method, implemented with the target ground-state RHF wave functions, is reliable in predicting a vast variety of the examined cross sections for single electron capture from multi-electron atomic targets by bare nuclei.

Acknowledgments

IM and NM thank the support by the Ministry of Education, Science and Technological Development of the Republic of Serbia: Project No. 171 020, whereas DD Project No. 176 021. DžB thanks two Research Funds: Radiumhemmet at the Karolinska University Hospital and the Stockholm Council City (FoUU).

Appendix

The quantities ν_i, ν_j, δ_i and δ_j from the main text are given by:

$$\nu_i = b_{-1}\mathcal{F}_i + 2b_0 D_i \mathcal{F}_i - 2b_1 D_i \mathcal{F}_i A_{\alpha_i}/\Delta_i, \tag{A.1}$$

$$\nu_j = a_{-1}\mathcal{F}_j + 2a_0 D_j \mathcal{F}_j - 2a_1 D_j \mathcal{F}_j A_{\alpha_j}/\Delta_j - 4a_2 D_j^2 \mathcal{F}_j A_{\beta_j}/\Delta_j, \tag{A.2}$$

$$\delta_i = 2b_0 D_i \mathcal{F}_i C_i + 2b_1 D_i \mathcal{F}_i B_{\alpha_i}/\Delta_i, \tag{A.3}$$

$$\delta_j = 2a_0 D_j \mathcal{F}_j C_j + 2a_1 D_j \mathcal{F}_j B_{\alpha_j}/\Delta_j + 4a_2 D_j^2 \mathcal{F}_j B_{\beta_j}/\Delta_j, \tag{A.4}$$

$$a_{-1} = 3Z_P t(5p_j - 1)/\Delta_j^2, \quad a_0 = 3Z_P t(5p_j - 1)/\Delta_j - 3p_j + 1, \tag{A.5}$$

$$a_1 = Z_P t(6p_j - 1) - \Delta_j(3p_j - 1), \quad a_2 = (Z_P t - \Delta_j)\Delta_j p_j, \tag{A.6}$$

$$b_{-1} = 3Z_P t/\Delta_i^2, \quad b_0 = 3Z_P t/\Delta_i - 1, \quad b_1 = Z_P t - \Delta_i, \tag{A.7}$$

$$\mathcal{F}_k = \frac{B_k^{i\xi}}{Q_1^2 + \Delta_k^2}, \quad B_k = \frac{2(v\Delta_k - i\vec{Q}_1 \cdot \vec{v})}{Q_1^2 + \Delta_k^2}, \quad (k = i, j), \tag{A.8}$$

$$C_k = \frac{v}{\Delta_k B_k} - 1, A_k = \frac{\Delta_k^2}{Q_1^2 + \Delta_k^2}, D_k = \frac{A_k}{\Delta_k}, \tag{A.9}$$

$$A_{\alpha_k} = 1 - 4A_k, B_{\alpha_k} = 1 + 2A_k C_{\alpha_k}, \quad C_{\alpha_k} = C_k[4 + (1 - i\xi)C_k], \tag{A.10}$$

$$A_{\beta_k} = 6[1 - 2A_k], B_{\beta_k} = 2A_k C_{\beta_k} + 3D_{\beta_k}, \quad D_{\beta_k} = 2 - (1 + i\xi)C_k, \tag{A.11}$$

$$C_{\beta_k} = C_k\{18 + 9(1 - i\xi)C_k + (1 - i\xi)(2 - i\xi)C_k^2\}. \tag{A.12}$$

ORCID iDs

D Delibašić https://orcid.org/0000-0003-3094-4304

References

[1] Cheshire I M 1964 *Proc. Phys. Soc. London* 84 89
[2] Janev R K, Presnyakov L P and Shevelko V P 1985 *Physics of Highly Charged Ions* (Berlin: Springer)
[3] Belkić Dž 2004 *Principles of Quantum Scattering Theory* (Bristol: Institute of Physics)
[4] Belkić Dž 2008 *Quantum Theory of High-Energy Ion-Atom Collisions* (London: Taylor & Francis)
[5] Belkić Dž (ed) 2013 *Fast Ion-Atom and Ion-Molecule Collisions* 1 (Singapore: World Scientific)
[6] Belkić Dž (ed) 2013 *Theory of Heavy Ion Collisions in Hadron Therapy* 65 (Amsterdam: Elsevier)
[7] Belkić Dž, Bray I and Kadyrov A (ed) 2019 *State-of-the-Art Reviews on Energetic Ion-Atom and Ion-Molecule Collisions* 2 (Singapore: World Scientific Publishing)
[8] Belkić Dž, Gayet R and Salin A 1979 *Phys. Rep.* **56** 279
[9] Belkić Dž, Mančev I and Hanssen J 2008 *Rev. Mod. Phys.* **80** 249
[10] Belkić Dž 2010 *J. Math. Chem.* **47** 1420
[11] Belkić Dž 2019 *J. Math. Chem.* **57** 1
[12] Belkić Dž, Gayet R, Hanssen J and Salin A 1986 *J. Phys.* B **19** 2945
[13] Belkić Dž and Taylor H S 1987 *Phys. Rev.* A **35** 1991
[14] Belkić Dž, Saini S and Taylor H S 1987 *Phys. Rev.* A **36** 1601
[15] Belkić Dž 1988 *Phys. Rev.* A **37** 55
[16] Belkić Dž 1988 *Eur. Phys. Lett.* **7** 323
[17] Belkić Dž 1989 *Phys. Scr.* **40** 610
[18] Belkić Dž and Mančev I 1990 *Phys. Scr.* **42** 285
[19] Belkić Dž 1993 *Phys. Rev.* A **47** 3824
[20] Belkić Dž 1993 *J. Phys.* B **26** 497
[21] Belkić Dž 1996 *Phys. Scr.* **53** 414
[22] Ghanbari-Adivi E and Bolorizadeh M A 2004 *J. Phys.* B **37** 3321
[23] Ghanbari-Adivi E and Velayati A N 2013 *Cent. Eur. J. Phys.* **11** 423
[24] Datta S K, Crothers D S F and McCarroll R 1990 *J. Phys.* B **23** 479
[25] Datta S 1992 *J. Phys.* B **25** 1001

[26] Mančev I, Milojević N and Belkić Dž 2019 *At. Data Nucl. Data Tables* **129-130** 101282
[27] Ermolaev A M 1984 *J. Phys.* B **17** 1069
[28] Ermolaev A M and Bransden B H 1984 *J. Phys.* B **17** 1083
[29] Ermolaev A M, Hewittt R N and McDowell M R C 1987 *J. Phys.* B **20** 3125
[30] Kirchner T, Lüdde H J and Dreizler R M 1999 *Phys. Rev.* A **61** 012705
[31] Kirchner T, Horbatsch M, Keim M and Lüdde H J 2004 *Phys. Rev.* A **69** 012708
[32] Martinez A E, Deco G R, Rivarola R D and Fainstein P D 1988 *Nucl. Instr. Meth.* B **34** 32
[33] Abufager P N, Martinez A E, Rivarola R D and Fainstein P D 2005 *Nucl. Instr. Meth.* B **233** 255
[34] Gravielle M S and Miraglia J E 1988 *Phys. Rev.* A **38** 5034
[35] Ghosh M, Mandal C R and Mukherjee S C 1987 *Phys. Rev.* A **35** 2815
[36] Mandal C R, Mandal M and Mukherjee S C 1990 *Phys. Rev.* A **42** 1803
[37] Winter T G 1993 *Phys. Rev.* A **47** 264
[38] Winter T G 1993 *Phys. Rev.* A **48** 3706
[39] Houamer S, Popov Yu V and Dal Cappello C 2009 *Phys. Lett.* A **373** 4447
[40] Crothers D S F and Dunseath K M 1987 *J. Phys.* B **20** 4115
[41] Marxer H and Briggs J S 1992 *J. Phys.* B **25** 3823
[42] Kuang Y R 1991 *Phys. Rev.* A **44** 1613
[43] Lin C D 1978 *J. Phys.* B **11** L185
[44] Shevelko V P 1978 *Z. Phys.* A **287** 19
[45] Janev R K, Presnyakov L P and Shevelko V P 1980 *Phys. Lett.* A **76** 121
[46] Mančev I, Milojević N and Belkić Dž 2018 *Eur. Phys. J.* D **72** 209
[47] Ghanbari-Adivi E and Ghavaminia H 2015 *Int. J. Mod. Phys.* E **24** 1550093
[48] Igarashi A and Lin C D 1999 *Phys. Rev. Lett.* **83** 4041
[49] Zou S, Pichl L, Kimura M and Kato T 2002 *Phys. Rev.* A **66** 042707
[50] Abdurakhmanov I B, Kadyrov A S, Avazbaev S K and Bray I 2016 *J. Phys.* B **49** 115203
[51] Avazbaev S K, Kadyrov A S, Abdurakhmanov I B, Fursa D V and Bray I 2016 *Phys. Rev.* A **93** 022710
[52] Abdurakhmanov I B, Bailey J J, Kadyrov A S and Bray I 2018 *Phys. Rev.* A **97** 032707
[53] Faulkner J, Abdurakhmanov I B, Alladustov Sh U, Kadyrov A S and Bray I 2019 *Plasma Phys. Control. Fusion* **61** 095005
[54] Roothaan C C J 1951 *Rev. Mod. Phys.* **23** 69
[55] Roothaan C C J 1960 *Rev. Mod. Phys.* **32** 179
[56] Clementi E and Roetti C 1974 *At. Data Nucl. Data Tables* **14** 177
[57] Koga T, Kanayama K, Watanabe S and Thakkar A J 1999 *Int. J. Quantum Chem.* **71** 491
[58] Koga T, Watanabe S, Kanayama K, Yasuda R and Thakkar A J 1995 *J. Chem. Phys.* **103** 3000
[59] Koga T, Tatewaki H and Thakkar A J 1994 *Theor. Chim. Acta* **88** 273
[60] Il'in R N, Oparin V A, Solov'ev E S and Fedorenko N V 1965 *Sov. Phys.-JETP Lett.* **2** 197
Il'in R N, Oparin V A, Solov'ev E S and Fedorenko N V 1967 *Sov. Phys.-Techn. Fiz.* **11** 921
Il'in R N, Oparin V A, Solov'ev E S and Fedorenko N V 1966 *Zh. Tekhn. Fiz.* **36** 1241
[61] DuBois R D and Toburen L H 1985 *Phys. Rev.* A **31** 3603
[62] Shah M B, Elliott D S and Gilbody H B 1985 *J. Phys.* B **18** 4245
[63] Grüebler W, Schmelzbach P A, König V and Marmier P 1970 *Helv. Phys. Acta* **43** 254
[64] D'yachkov B A 1968 *Zh. Tekhn. Fiz.* **38** 1259
[65] Sasao M, Sato K, Matsumoto A, Takagi S, Amemiya S, Masuda T, Tsurita Y, Fukuzawa F, Haruyama Y and Kanamori Y 1986 *J. Phys. Soc. Japan* **55** 102
[66] McCullough R W, Goffe T V, Shah M B, Lemon N and Gilbody H B 1982 *J. Phys.* B **15** 111
[67] Murray G A, Stone J, Mayo M and Morgan T J 1982 *Phys. Rev.* A **25** 1805
[68] Rødbro M, Horsdal-Pedersen E, Cocke C L and Macdonald J R 1979 *Phys. Rev.* A **19** 1936
[69] Cocke C L, Gardner R K, Curnutte B, Bratton T and Saylor T K 1977 *Phys. Rev.* A **16** 2248
[70] Acerbi E, Castiglioni M, Dutto G, Resmini F, Succi C and Tagliaferri G 1967 *N. Cim.* B **50** 176
[71] Acerbi E, Candoni B, Castiglioni M, Dutto G, Fait G, Resmini F and Succi C 1969 *N. Cim.* A **64** 1068
[72] Shryber U 1967 *Helv. Phys. Acta* **40** 1023
[73] Welsh L M, Berkner K H, Kaplan S N and Pyle R V 1967 *Phys. Rev.* **158** 85
[74] Toburen L H, Nakai M Y and Langley R A 1968 *Phys. Rev.* **171** 114
[75] Berkner K H, Kaplan S N, Paulikas G A and Pyle R V 1965 *Phys. Rev.* **140** A729
[76] Allison S K 1958 *Rev. Mod. Phys.* **30** 1137
[77] Varghese S L, Bissinger G, Joyce J M and Laubert R 1985 *Phys. Rev.* A **31** 2202
[78] Katayama I, Berg G P A, Hurlimann W, Martin S A, Meissburger J, Oelert W, Rogge M, Romer J G M, Tain J L, Zemlo L and Gaul G 1984 *J. Phys.* B **17** L23